Unsteady Local Linearization Solution for Pitching Bodies of Revolution at $M_\infty = 1$: Stability Derivative Analysis

Stephen S. Stahara*
Nielsen Engineering & Research, Inc., Mountain View, Calif.
and
John R. Spreiter†
Stanford University, Stanford, Calif.

An account is provided of recent theoretical results for unsteady inviscid transonic flows about axisymmetric bodies. The unsteady local linearization solution is developed to calculate the unsteady pressure distributions, for sonic or near-sonic freestream flows, on the surface of several slender, pointed, axisymmetric bodies undergoing low-frequency oscillatory pitching motion. Results determined for static and dynamic stability derivatives exhibit good agreement with the limited experimental data available.

Introduction

THE purpose of this paper is to describe a theoretical procedure for determining the unsteady flowfield at freestream Mach numbers at or near one about slender axisymmetric bodies undergoing oscillatory pitching motion. The analysis is based on the small-disturbance theory of inviscid unsteady transonic flow and makes use of the concept of splitting the flow into steady and unsteady components and solving the resultant unsteady potential equation by the local linearization technique. An expansion of the unsteady solution is obtained for low reduced frequencies, for which the nonlinear thickness and Mach number effects of the steady flow are significant, and the Adam-Sears iteration procedure is used to determine the unsteady near-field potential, from which flow properties on the body surface are calculated. The approach generalizes the results of Landahl,[1] Liu,[2] Liu et al.,[3] and Ruo and Liu,[4] both in the sense of encompassing the entire low-frequency range, including $k=0$, and also in eliminating the "parabolic" assumption,[3,4] thereby properly accounting for local regions of subsonic, sonic, and supersonic flow. Applications are made to various parabolic-arc half-bodies and cones at $M_\infty = 1$, and results are presented for unsteady force and moment distributions and static and dynamic stability derivatives. The examples were selected, insofar as possible, to enable comparison with existing data and other theories. We note that alternative approaches, employing the recently developed methods of Isogai[5] and Dowell,[6] that are based on the same general notions of the local linearization method are also possible and would provide an interesting further comparison of these different procedures.

Analysis

Basic Equations

The analysis is developed in terms of a body-fixed cylindrical coordinate system centered at the nose with the x axis directed rearward and aligned with the longitudinal axis of the body, and the $\theta = 0$ deg axis directed to the right, facing forward. A slender, pointed body of revolution immersed in a zero angle-of-attack steady flow is assumed to undergo small-amplitude harmonic pitching oscillations about a point located on the body axis at $x=a$. With the fundamental assumption that the body is sufficiently smooth and slender so that the inviscid small disturbance theory applies, a perturbation velocity potential ϕ may be defined according to[7]

$$\phi(x,r,\theta,t) = U_\infty [\,(x-a)\ \cos\delta + r\ \sin\theta\ \sin\delta + \phi(x,r,\theta,t)\,] \tag{1}$$

where U_∞ represents the freestream velocity. The angular displacement $\delta(t)$ is given by

$$\delta(t) = RP[\delta_0 e^{ikt}] \tag{2}$$

where δ_0 is the maximum displacement, RP signifies the real part of a complex quantity, k is the reduced frequency defined by $k=\omega\ell/U_\infty$, and ϕ satisfies

$$(1-M_\infty^2)\phi_{xx} + \phi_{rr} + \frac{1}{r}\phi_r + \frac{1}{r^2}\phi_{\theta\theta} = M_\infty^2(\gamma+1)\phi_x\phi_{xx} + M_\infty^2\phi_{tt} + 2M_\infty^2\phi_{xt} \tag{3}$$

In Eq. (3), M_∞ is the freestream Mach number; (x,r,θ) are nondimensional body-fixed cylindrical coordinates with (x,r) normalized by body length ℓ; t is nondimensional time normalized by ℓ/U_∞; and γ is the ratio of specific heats equal to 7/5 for air.

For the oscillatory flows considered here, it is convenient to expand the solution into a steady and unsteady component. Thus, we set

$$\phi(x,r,\theta,t) = \phi_1(x,r) + RP[\tilde{\phi}(x,r)\ \sin\theta e^{ikt}] \tag{4}$$

where ϕ_1 is the axisymmetric steady perturbation potential, which satisfies Eq. (3) with the (θ,t) terms omitted, and ϕ is the complex amplitude of the oscillatory perturbation velocity potential. On the assumption of small amplitude oscillations appropriate for flutter and stability analysis, the equation for ϕ becomes

$$\tilde{\phi}_{rr} + \frac{1}{r}\tilde{\phi}_r - \frac{1}{r^2}\tilde{\phi} = [M_\infty^2 - 1 + M_\infty^2(\gamma+1)\phi_{1x}]\tilde{\phi}_{xx} + \tilde{M}_\infty^2(\gamma+1)\phi_{1_{xx}} + 2ikM_\infty^2]\tilde{\phi}_x - M_\infty^2 k^2\tilde{\phi} \tag{5}$$

Received Feb. 23, 1976; revision received June 23, 1976. This work was supported by the Office of Naval Research under Contract N00014-73-C-0379.

Index categories: Nonsteady Aerodynamics, Subsonic and Transonic Flow.

*Senior Research Scientist. Member AIAA.

†Professor, Departments of Aeronautics and Astronautics and of Mechanical Engineering. Consultant to Nielsen Engineering & Research, Inc. Fellow AIAA.

which, although being linear, is formidable to solve because of the variable coefficients and mixed elliptic-hyperbolic type.

The boundary condition of flow tangency at the body surface can be decomposed analogously. In the body-fixed coordinate system, these conditions are[7]

$$\phi_{1_r}(x,R) = R' + 0(\epsilon^3 \ln\epsilon) \tag{6a}$$

$$\tilde{\phi}_r(x,R) = \delta_0[1 + k(x-a)] + R'\tilde{\phi}_x(x,R) - ik\delta_0 RR' + 0(\delta_0\epsilon^4 \ln\epsilon, \delta_0^2) \tag{6b}$$

where $R = \epsilon\bar{R}(x)$ describes the body ordinates. Here, ϵ is the normalized maximum body thickness, and $\bar{R}$ is a function of order one. At infinity, the perturbation potentials are required to vanish in an appropriate manner. Since attention will be confined to flows with $M_\infty \approx 1$ having all shock waves downstream of the region for which results will be calculated, we will not require the corresponding relation for conditions on the two sides of a shock wave. The preceding equations provide, therefore, the fundamental relations for the analysis to follow.

Local Linearization Solution

The differential equation (5) for the unsteady component can be expressed in the compact form

$$\lambda_1\tilde{\phi}_{xx} + \lambda_2\tilde{\phi}_x + \lambda_3\tilde{\phi} = \tilde{\phi}_{rr} + \frac{1}{r}\tilde{\phi}_r - \frac{1}{r^2}\tilde{\phi} \tag{7}$$

where

$$\lambda_1 = M_\infty^2 - 1 + M_\infty^2(\gamma+1)\phi_{1x}, \qquad \lambda_2 = M_\infty^2(\gamma+1)\phi_{1xx} + i2kM_\infty^2, \qquad \lambda_3 = -k^2M_\infty^2$$

Three fundamentally different differential equations and solutions occur for $\tilde{\phi}$ depending upon whether the coefficient λ_1, which corresponds in the small-disturbance approximation to $M_{\text{local}}^2 - 1$, is negative, near zero, or positive.[8] The zone of influence of each solution is different for each case, as is appropriate since they correspond to local regions of subsonic, sonic, or supersonic flow. Each solution then forms the basis of the ensuing analysis in its appropriate region, with the requirement that each partial solution is required to merge continuously with that for the adjacent region. The local linearization method proceeds by replacing temporarily the variable coefficients (λ_1, λ_2) in Eq. (7) by constants and solving the simplified equations that result in each of the three regions discussed above. Next, the quantities $\tilde{\phi}_x(x,R)$ and $\tilde{\phi}(x,R)$, which are required for evaluating surface properties of the flow, such as the unsteady pressure coefficient, are determined by first obtaining them from the simplified equations, then replacing the constants (λ_1, λ_2) by the functions they originally represented, and finally evaluating the resulting expressions at points along the body.

The three starting solutions for $\tilde{\phi}$ are given by

$$\underset{\text{sonic}}{\tilde{\phi}(x,r)} = \frac{1}{2}\frac{\partial}{\partial r}\int_0^x \frac{g(\xi)\ \exp\left[-A_0(x-\xi) - \dfrac{\lambda_2 r^2}{4(x-\xi)}\right]}{x-\xi}\,d\xi \quad (\lambda_1 \simeq 0) \tag{8}$$

$$\underset{\text{subsonic}}{\tilde{\phi}(x,r)} = \frac{1}{2}\frac{\partial}{\partial r}\int_0^l \frac{g(\xi)\ \exp[-A_1(x-\xi) + A_2[(x-\xi)^2 + (-\lambda_1)r^2]^{1/2}]}{[(x-\xi)^2 + (-\lambda_1)r^2]^{1/2}}\,d\xi \quad (\lambda_1 < 0) \tag{9}$$

$$\underset{\text{supersonic}}{\tilde{\phi}(x,r)} = \frac{1}{2}\frac{\partial}{\partial r}\int_0^{x-\sqrt{\lambda_1}r} \frac{g(\xi)\exp[-A_1(x-\xi)]\cosh[A_2[A_2[(x-\xi)^2 - \lambda_1 r^2]^{1/2}]}{[(x-\xi^2 - \lambda_1 r^2]^{1/2}}\,d\xi \quad (\lambda_1 > 0) \tag{10}$$

where $g(x)$ is the doublet strength to be determined later from the boundary condition,

$$A_0 = \lambda_3/\lambda_2, \qquad A_1 = \lambda_2/2\lambda_1, \qquad \text{and} \quad A_2 = \sqrt{\lambda_2^2 - 4\lambda_1\lambda_3}\ /2\lambda_1$$

In determining the local linearization solution, the forms of these solutions in the near field are required. These could be obtained by expanding the above solutions directly for small r; however, a more convenient method is to Fourier transform the basic equation (7) for the three different regions with respect to x, solve the transformed equations, expand the Kernel functions in the transformed solutions for small r, and then transform the simplified results back to the physical plane. Use of either technique leads, after much manipulation, to the following forms:

$$\underset{\text{sonic}}{\tilde{\phi}(x,r)} = -\left[\frac{g(x)}{r} + \frac{r}{4}\left\{\Lambda(x)\left[E_{in}(A_0x) + \ln\left(\frac{\lambda_2 r^2}{4x}\right) + C - 1\right]\right.\right.$$

$$\left.\left. + \int_0^x \frac{\Lambda(x) - \Lambda(\xi)}{x-\xi} e^{-A_0(x-\xi)}\,d\xi - \lambda_2 g(0)\frac{e^{-A_0x}}{x}\right\}\right] + 0(r^3\ln r) \quad (\lambda_1 \simeq 0) \tag{11}$$

$$\underset{\text{subsonic}}{\tilde{\phi}(x,r)} = -\left[\frac{g(x)}{r} + \frac{r}{4}\left\{\Lambda(x)\left\{E_{in}(A_3x) + E_{in}[-A_4(1-x)] + \ln\left[\frac{-\lambda_1 r^2}{4x(1-x)}\right] - 1\right\}\right.\right.$$

$$+ \int_0^x \frac{\Lambda(x) - \Lambda(\xi)}{x-\xi} e^{-A_3(x-\xi)}d\xi - \int_x^1 \frac{\Lambda(\xi) - \Lambda(x)}{\xi - x} e^{A_4(\xi - x)}\,d\xi$$

$$\left.\left. + \left\{\left[\lambda_1\left(\frac{1}{x} + A_3\right) - \lambda_2\right]g(o) - \lambda_1 g'(o)\right\}\frac{e^{-A_3x}}{x} + \left\{\left[\lambda_1\left(\frac{1}{1-x} - A_4\right) + \lambda_2\right]g(1) + \lambda_1 g'(o)\right\}\frac{e^{A_4(1-x)}}{1-x}\right\}\right] + 0(r^3\ln r) \quad (\lambda_1 < o) \tag{12}$$

$$\underset{\text{supersonic}}{\tilde{\phi}(x,r)} = -\left[\frac{g(x)}{x} + \frac{r}{4}\left\{\Lambda(x)\left[E_{in}(A_3 x) + E_{in}(A_4) + \ln\left(\frac{\lambda_1 r^2}{4x^2}\right) - 1\right] + \int_0^x \frac{\Lambda(x)-\Lambda(\xi)}{x-\xi}\left[e^{-A_3(x-\xi)} + e^{-A_4(x-\xi)}\right]d\xi\right.\right.$$

$$\left.\left. + \left\{\left[\lambda_1\left(\frac{1}{x}+A_3\right)-\lambda_2\right]e^{-A_3 x} + \left[\lambda_1\left(\frac{1}{x}+A_4\right)-\lambda_2\right]e^{-A_4 x}\right\}\frac{g(o)}{x} - \lambda_1\left(e^{-A_3 x}+e^{-A_4 x}\right)\frac{g'(o)}{x}\right\}\right] + O(r^3 \ln r) \quad (\lambda_1 > 0) \tag{13}$$

where

$$\Lambda(x) \equiv \lambda_1 g''(x) + \lambda_2 g'(x) + \lambda_3 g(x)$$

$E_{in}(Z)$ is the complete exponential function of complex argument Z[9], $C = 0.577216$ is Euler's constant,

$$A_3 = (\lambda_2 - \sqrt{\lambda_2^2 - 4\lambda_1\lambda_3})/2\lambda_1,$$

and

$$A_4 = (\lambda_2 + \sqrt{\lambda_2^2 - 4\lambda_1\lambda_3})/2\lambda_1$$

Low Frequency Solution

Of primary importance in this investigation are low frequency oscillations, that is, $k = 0(\epsilon^2 \ln\epsilon)$, where the nonlinear thickness and Mach number effects of the steady flow strongly influence the unsteady flow. For this frequency regime, it is convenient to decompose the unsteady component in the following manner

$$\tilde{\phi}(x,r)e^{ikt} = \delta\tilde{\phi}^i(x,r) + \dot{\delta}\tilde{\phi}^o(x,r) \tag{14}$$

where $\dot{\delta} = ik\delta$ and the superscripts (i,o) denote, respectively, the in-phase and out-of-phase unsteady components.

What remains now is to obtain to appropriate order the doublet distribution $g(x)$ appearing in Eqs. (11-13). An effective means employed in similar investigations[1-4] is to make use of the Adam-Sears technique. If we represent the doublet distribution and potential by

$$g(x) = g_1(x) + g_2(x) \tag{15}$$

$$\tilde{\phi}^{i,o}(x,r) = \tilde{\phi}_1^{i,o}(x,r) + \tilde{\phi}_2^{i,o}(x,r) \tag{16}$$

where $g_1(x)$ and $\tilde{\phi}_1^{i,o}(x,r)$ represent the first-order effects, whereas $g_2(x)$ and $\tilde{\phi}_2^{i,o}(x,r)$ are of a higher unspecified order, application of the surface boundary condition equation (6) serves to determine the distributions (g_1, g_2) explicitly, and, from these, the solution for the near-field potential follows directly. The result of these operations-after taking into account that $\lambda_1 = 0(\epsilon^2\ln\epsilon), \lambda_2 = 0(\epsilon^2\ln\epsilon) + 0(k), \lambda_3 = 0(k^2), \dot{\delta} = ik\delta$, ignoring $0(k^2)$ terms, and retaining terms in the near-field potentials to $0(\epsilon^3, \epsilon^3\ln\epsilon)$ as is consistent with the boundary condition equation (6) – is that $g_1 = 0(\epsilon^2), \tilde{\phi}_1^{i,o} = 0(\epsilon^2/r)$ represent the slender-body doublet, whereas $g_2 = 0(\epsilon^4, \epsilon^4 \ln\epsilon), \tilde{\phi}_2^{i,o} = 0(\epsilon^4/r, \epsilon^2 r \ln r, \epsilon^2 r)$ represent the second-order correction due to body thickness, reduced frequency, and Mach number. Specifically, we find that

$$\begin{Bmatrix}\tilde{\phi}^i \\ \tilde{\phi}^o\end{Bmatrix} = \begin{Bmatrix}\tilde{\phi}_1^i(x,r) \\ \tilde{\phi}_1^o(x,r)\end{Bmatrix} + \begin{Bmatrix}\tilde{\phi}_2^i(x,r) \\ \tilde{\phi}_2^o(x,r)\end{Bmatrix} + O(\epsilon^4 \ell n\epsilon) \text{ for } r = O(\epsilon) \tag{17}$$

where

$$\begin{Bmatrix}\tilde{\phi}_1^i \\ \tilde{\phi}_1^o\end{Bmatrix} = \begin{Bmatrix}1 \\ x-a\end{Bmatrix}\frac{Q(x)}{\pi r} \tag{18}$$

and

$$\tilde{\phi}_2^i = -\frac{Q'^2(x)}{4\pi^2 r} \tag{19}$$

$$\underset{\text{sonic}}{\tilde{\phi}_2^o(x,r)} = \frac{1}{4\pi}\left[\frac{Q(x)}{\pi r} + r\right]\left[2M_\infty^2\left\{Q'(x)\left[\ln\left(\frac{|\lambda_2|}{4x}\right) + C + 1 + \frac{\tan^{-1}\left(\frac{2kM_\infty^2}{\lambda_{2RP}}\right)}{\left(\frac{2kM_\infty^2}{\lambda_{2RP}}\right)}\right] + \int_0^x \frac{Q'(x)-Q'(\xi)}{x-\xi}d\xi\right\}\right] + \Delta\tilde{\phi}(x,r) \tag{20}$$

$$\underset{\text{subsonic}}{\tilde{\phi}_2^o(x,r)} = \frac{1}{4\pi}\left[\frac{Q(x)}{\pi r} + r\right]\left[2M_\infty^2\left(Q'(x)\left\{E_{in}\left[-\frac{\lambda_2}{\lambda_1}(1-x)\right]_{RP} + \ln\left[-\frac{\lambda_1}{4x(1-x)}\right] + 1\right\} + \int_0^x \frac{Q'(x)-Q'(\xi)}{x-\xi}d\xi\right.\right.$$

$$\left. - \int_0^1 \frac{Q'(\xi)-Q'(x)}{\xi-x}\left[e^{(\lambda_2/\lambda_1)(\xi-x)}\right]_{RP}d\xi\right) + \left[\lambda_1 Q''(x) + \lambda_{2_{RP}}Q'(x)\right]\left\{\frac{E_{in}\left[-\frac{\lambda_2}{\lambda_1}(1-x)\right]}{k}\right\}_{IP}$$

$$\left. + \int_x^1 \frac{\lambda_1[Q''(\xi)-Q''(x)] + \lambda_{2RP}[Q'(\xi)-Q'(x)]}{\xi-x}\left[\frac{e^{(\lambda_2/\lambda_1)(\xi-x)}}{k}\right]_{IP}d\xi + \frac{\lambda_1}{(1-x)}\left[\frac{Q(x)}{1-x} + Q'(1)\right]\left[\frac{e^{(\lambda_2/\lambda_1)(1-x)}}{k}\right]_{IP}\right] + \Delta\tilde{\phi}(x,r) \tag{21}$$

$$\tilde{\phi}_2^o(x,r)_{\text{supersonic}} = \frac{1}{4\pi}\left[\frac{Q(x)}{\pi r}+r\right]\left[2M_\infty^2\left\{Q'(x)\left[E_{in}\left(\frac{\lambda_2}{\lambda_1}x\right)_{RP}+\ln\left(\frac{\lambda_1}{4x^2}\right)+1\right]\right.\right.$$

$$+\int_0^x \frac{Q'(x)-Q'(\xi)}{x-\xi}\left[1+e^{-(\lambda_2/\lambda_1)(x-\xi)}\right]_{RP}d\xi\Bigg\}+\Bigg[\lambda_1 Q''(x)$$

$$\left.\left.+\lambda_{2_{RP}}Q'(x)\right]\left[\frac{E_{in}\left(\frac{\lambda_2}{\lambda_1}x\right)}{k}\right]_{IP}+\int_0^x\frac{\lambda_1[Q''(x)-Q''(\xi)]+\lambda_{2RP}[Q'(x)-Q'(\xi)]}{x-\xi}d\xi\right]+\Delta\tilde{\phi}(x,r) \tag{22}$$

where

$$\Delta\tilde{\phi}(x,r) = -\frac{(x-a)Q'^2(x)}{4\pi^2 r}+\frac{M_\infty^2 Q'(x)}{2\pi}\left[\frac{Q(x)}{\pi r}\ln\frac{Q(x)}{\pi}+r\ln r^2\right] \tag{23}$$

In Eqs. (20) to (22), the coefficients (λ_1,λ_2) are evaluated on the body surface $r=R$ and, consequently, are functions of x only,

$$\lambda_{2_{RP}} = RP(\lambda_2) = M_\infty^2(\gamma+1)\phi_{1_{xx}}(x,R) \tag{24}$$

$Q(x)$ represents the body area distribution, and is given by $Q(x)=\pi R^2(x)$ and IP signifies the imaginary part of a complex quantity. Also, implicit in those equations are the appropriate limiting forms as $k\to 0$. For example,

$$\lim_{k\to 0}\left[\frac{\tan^{-1}\left(\frac{2kM_\infty^2}{\lambda_{2RP}}\right)}{\left(\frac{2kM_\infty^2}{\lambda_{2RP}}\right)}\right]=1+0(k^2) \tag{25}$$

$$\lim_{k\to 0}\left\{\frac{E_{in}\left[-\frac{\lambda_2}{\lambda_1}(1-x)\right]}{k}\right\}_{IP}=\frac{2M_\infty^2}{\lambda_{2RP}}\left[1-e^{(\lambda_{2RP})\lambda_1(1-x)}\right]+0(k^2) \tag{26}$$

We note that the present sonic region results are in agreement with the low-frequency parabolic-method results of Refs. 3 and 4 when several higher order terms (in ϵ) inconsistently included in those results are omitted. With $\tilde{\phi}(x,r)$ known, the surface pressure coefficient can be determined for low-frequency, small-amplitude oscillations from the result[7] that

$$C_p(x,R,\theta,t) = C_{p_1}(x,R)+[\delta\tilde{C}_p^i(x,R)+\delta\tilde{C}_p^o(x,R)]\sin\theta \tag{27}$$

where the steady pressure coefficient is given by

$$C_{p_1}(x,R) = -2\phi_{1_x}(x,R)-R'^2 \tag{28}$$

while the in-phase and out-of-phase unsteady pressures are

$$\tilde{C}_p^i(x,R) = -2\tilde{\phi}_{1_x}^i(x,R)+2\left\{[(1-M_\infty^2)\phi_{1_x}(x,R)-\left(1-\frac{M_\infty^2}{2}\right)R'^2]\tilde{\phi}_{1_x}^i(x,R)-\tilde{\phi}_{2_x}^i(x,R)\right\}=\tilde{C}_{p_1}^i(x,R)+\tilde{C}_{p_2}^i(x,R) \tag{29}$$

$$\tilde{C}_p^o(x,R) = -2[\tilde{\phi}_{1_x}^o(x,R)+\tilde{\phi}_1^i(x,R)]+2\left\{\left[(1-M_\infty^2)\phi_{1_x}(x,R)-\left(1-\frac{M_\infty^2}{2}\right)R'^2\right]\tilde{\phi}_{1_x}^o(x,R)\right.$$

$$\left.+[M_\infty^2\phi_{1_x}(x,R)+\frac{1}{2}M_\infty^2R'^2]\tilde{\phi}_1^i(x,R)+R\phi_{1_x}(x,R)+RR'^2-\tilde{\phi}_{2_x}^o(x,R)-\tilde{\phi}_2^i(x,R)\right\}=\tilde{C}_{p_1}^o(x,R)+\tilde{C}_{p_2}^o(x,R) \tag{30}$$

where $(\tilde{C}_{P_1}^{i,o}\ \tilde{C}_{P_2}^{i,o}$ represent, respectively, the first- and second-order unsteady pressure coefficients. From these, the flutter and stability derivatives can be calculated directly using

$$\begin{Bmatrix}C_{M_\delta}\\ C_{M_{\dot\delta}}\end{Bmatrix}_{1,2}=-\frac{1}{\epsilon^2}\int_0^1\left[(x-a)\begin{Bmatrix}\tilde{C}_p^i(x,R)\\ \tilde{C}_p^o(x,R)\end{Bmatrix}_{1,2}+R(x)R'(x)\begin{Bmatrix}\tilde{C}_p^i(x,R)\\ \tilde{C}_p^o(x,R)\end{Bmatrix}_1\right]dx$$

$$\begin{Bmatrix}C_{N_\delta}\\ C_{N_{\dot\delta}}\end{Bmatrix}_{1,2}=-\frac{1}{\epsilon^2}\int_0^1 R(x)\begin{Bmatrix}C_p^i(x,R)\\ C_p^o(x,R)\end{Bmatrix}_{1,2}dx \tag{31}$$

where again the subscripts (1,2) serve to identify the first-and second-order components of the various derivatives.

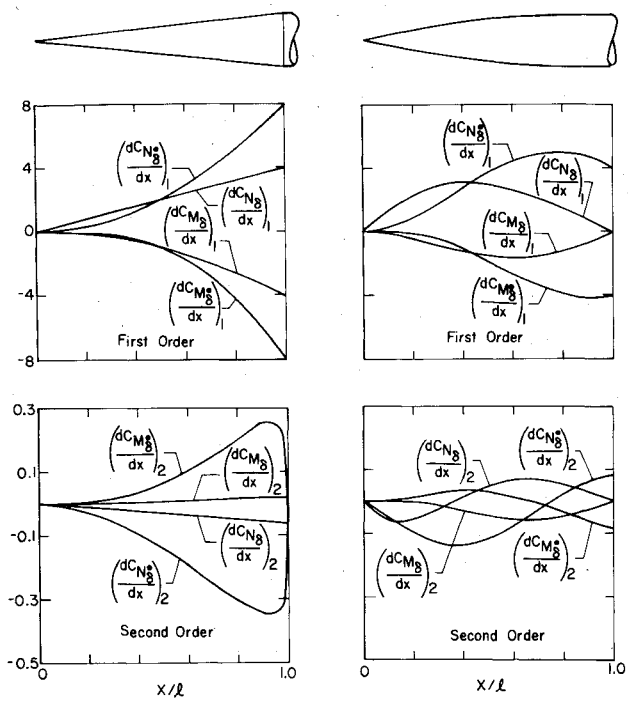

Fig. 1 Distributions of first- and second-order flutter derivatives for a cone and a parabolic half-body with $\epsilon = 0.1$ oscillating in pitch about $a = 0$ at $M_\infty = 1$.

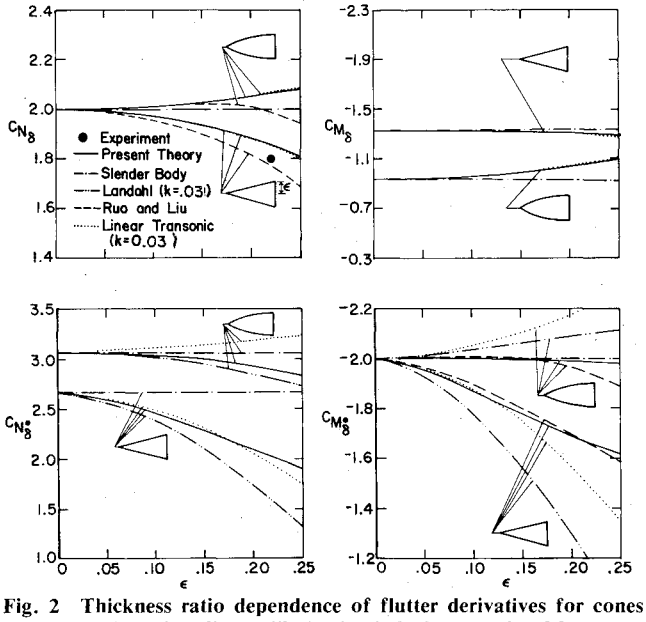

Fig. 2 Thickness ratio dependence of flutter derivatives for cones and parabolic half-bodies oscillating in pitch about $a = 0$ at $M_\infty = 1$.

Results

In order to demonstrate the effects of thickness ratio, reduced frequency, pitch axis location, and body geometry on the unsteady motion, the results of the previous analysis were applied to various finite-length circular cones and parabolic-arc half-bodies described, respectively, by

$$\left.\begin{aligned} R(x) &= \epsilon x \\ R(x) &= \epsilon(2x - x^2) \end{aligned}\right\} \quad 0 \le x \le l \tag{32}$$

Static and dynamic flutter derivations, as well as their variation along the body surface, were calculated for $M_\infty = 1$. In the results presented, the steady-state solutions required as input to the unsteady calculations were determined by the

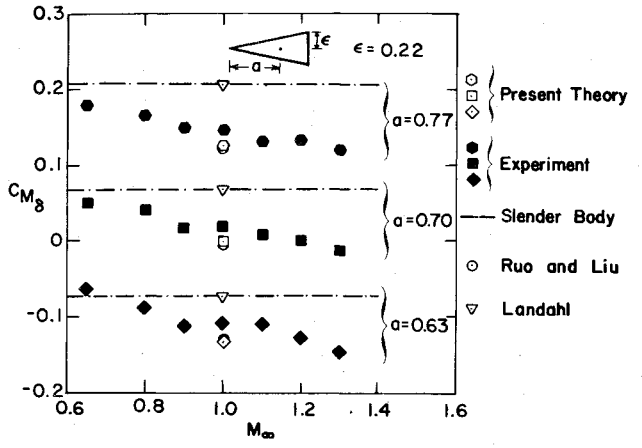

Fig. 3 Pitch moment flutter derivative for a 12.5 deg half-angle cone at $M_\infty = 1$.

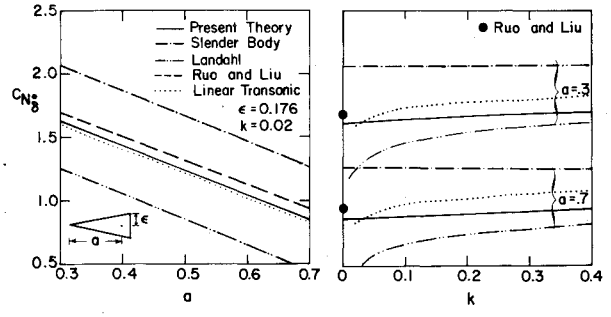

Fig. 4 Pitch axis and frequency dependence of damping-in-pitch normal-force coefficient of a 10 deg half-angle cone at $M_\infty = 1$.

local linearization method,[10] which is known to provide results of good accuracy for the shapes considered here.

Figure 1 exhibits in the left-hand plots the distributions of the first- and second-order static $(dC_{N_\delta}/dx, dC_{M_\delta}/dx)_{1,2}$ and dynamic $(dC_{N_\delta}/dx, dC_{M_\delta}/dx)_{1,2}$ flutter derivatives for a cone having a maximum thickness $\epsilon = 0.1$ undergoing slow oscillations in pitch about its nose at $M_\infty = 1$. We note in particular the rapid variation of the second-order dynamic derivatives $(dC_{N_\delta}/dx, dC_{M_\delta}/dx)_2$ in the vicinity of the shoulder, a result of the logarithmic behavior of the steady-state solution[10] in that region. Analogous results for a parabolic-arc half-body are given in the right-hand plots. No large gradients are present in those results, but, as expected, a smooth variation is indicated of the various derivatives along the entire length of the body. The parabolic-arc results for the second-order distributions of normal force $(dC_{N_\delta}/dx)_2$ and damping-in-pitch normal force $(dC_{N_\delta}/dx)_2$ presented here agree in trend but differ somewhat in magnitude with those determined by the "parabolic" method.[3] Those results would correspond to using the sonic results of the present method over the entire body with the additional provision that the surface acceleration [see Eq. (24)] is held constant at some representative value.[10]

Figure 2 provides the thickness-ratio dependence of the present theory for the static $(C_{N_\delta}, C_{M_\delta})$ and dynamic $(C_{N_\delta}, C_{M_\delta})$ flutter derivatives for both cones and parabolic-arc half-bodies oscillating in pitch about the nose at the reduced frequency $k = 0.03$ and $M_\infty = 1$. Also shown for comparison are various available theoretical and experimental results. These include the results of Landahl,[1] the linear transonic method of Liu,[2] the "parabolic" method of Ruo and Liu,[4] and the results of slender body theory, together with experimental data of Wehrend[11] for the normal-force coefficient slope C_{N_δ} of a 12.5 deg half-angle cone with a flat base. Considering first the static derivative comparisons shown in the two upper plots, we note that Landahl's results for

$(C_{N_\delta}, C_{M_\delta})$ are only first order in thickness ratio and consequently identical to slender-body theory. The linear transonic theory results of Liu[2] for $(C_{N_\delta}, C_{M_\delta})$ are identical to the present results for zero frequency; however, those results contain in addition terms linear in k that, for the frequency regime considered here, are of higher order and do not enter into the present results. Comparison with results of the "parabolic" method of Ruo and Liu[4] for C_{N_δ} indicate considerable discrepancy from the present results as the thickness ratio increases and presumably is due to the inconsistent inclusion of higher order terms $0(\epsilon^6 \ln\epsilon/r, r\epsilon^4 \ln\epsilon)$ in that calculation. For the dynamic derivative comparisons shown in the two lower plots, large discrepancies and different trends exist among the various theories. Because Landahl's results are based upon a lower order surface boundary condition, as well as a less accurate force and moment determination, those results can be expected to deviate from the more exact treatment used in the present analysis and those of Liu[2] and Ruo and Liu[4] as the thickness ratio increases. With regard to the comparisons of the linear transonic theory results of Liu,[2] we note that, for the parabolic-arc half-bodies, the failure of that theory to include the effect of the nonlinear steady flow on the unsteady problem is sufficient to change the entire trend of the dependence of the dynamic stability derivatives on thickness ratio. This provides yet another example of both the sensitivity and dependence of the unsteady motion on the nonlinear steady flow at transonic speeds and points out the necessity of including this effect.

A final comparison of static derivative results of the present method with experiment is provided in Fig. 3. Here, the data obtained by Wehrend[11] for the slope of the pitching moment coefficient C_{M_δ} is shown for a 12.5 deg half-angle cone for three different pitch axes locations at, respectively, 63 percent, 70 percent, and 77 percent of the body length from the nose and for freestream Mach numbers from 0.65 to 1.30. Also provided are the theoretical results of the present method for $M_\infty = 1$, as well as those of Landahl,[1] Ruo and Liu,[4] and slender-body theory. We note again that the linear transonic theory results of Liu[2] for the static derivatives are essentially identical to the present theory and have been omitted for clarity of presentation. Good agreement of the present results is noted with both experiment and the "parabolic" results of Ruo and Liu.[4]

Figure 4 displays the pitch axis and frequency dependence predicted by the present method for the damping-in-pitch normal-force coefficient C_{N_δ} of a 10 deg half-angle cone oscillating in pitch at $M_\infty = 1$. Shown for comparison are the results of Landahl,[1] the linear transonic method of Liu,[2] the "parabolic" method used by Ruo and Liu,[4] and slender-body theory. Significant differences among the various results are observed. Moreover, the well-known logarithmic singularity predicted both by Landahl's method[1] and linear transonic theory[2] as the reduced frequency $k \to 0$ is quite evident, and is in distinct contrast to the smooth variation with k of the present theory. Moreover, we note that the results of Ruo and Liu,[4] which are valid only for very low (quasisteady) frequencies and which do not contain an explicit dependence on k, compare favorably with the present theory near $k = 0$.

A further comparison of the results for the damping-in-pitch normal-force coefficient is provided in Fig. 5, which displays the influence of body shape on both the pitch axis and frequency dependence of C_{N_δ}. Here, various theoretical results for a cone are shown in the two upper plots and are contrasted in the lower plots with the results for a parabolic-arc half-body having the same normalized maximum thickness $\epsilon = 0.10$. Greater disagreement exists among the results of the various theories for the conical rather than the parabolic-arc shape, a fact already observed in the thickness-ratio comparisons of $(C_{N_\delta}, C_{M_\delta})$ shown in Fig. 2. This is almost certainly a result of the particular behavior of the flow in the vicinity of the shoulder of conical bodies, where rapid variations in flow properties occur – an effect altogether absent in the smoothly continuous flow about parabolic-arc half-bodies.

Results analogous to those given in Fig. 4 and 5 are presented in Figs. 6 and 7 for the damping-in-pitch moment coefficient C_{M_δ}. In Fig. 6, results for the damping-in-pitch moment coefficient C_{M_δ} of a 12.5 deg half-angle cone at $M_\infty = 1$ are exhibited. In addition to the theoretical results indicated, experimental data of Wehrend[11] for pitch axes locations $a = 0.63$, 0.70, and 0.77 are also included in the plot on the left. We note that although the present theory provides results somewhat closer to the data than the other methods, none of the theoretical results can be considered to be in acceptable agreement with the data. A feature that introduces additional uncertainty into these comparisons is that the actual flow past a cone with flat base will contain a free streamline emanating from the shoulder whose predicted location is beyond the scope of an inviscid theory. Whereas the direction of that streamline will undoubtedly be close to freestream and its influence restricted essentially to the vicinity of the cone shoulder, inviscid theory predicts that the surface pressures will be unaffected by this feature of the flow, as the influence of its effect is limited to regions of the flow field downstream of the limiting characteristic emanating from the cone shoulder. Discrepancies associated with this effect, together with other uncertainties related to the dynamic testing,[11] are difficult to assess further without additional experiment and analysis. With regard to Fig. 6, we observe again the differences between the various methods, particularly as shown in the plot on the right at low frequen-

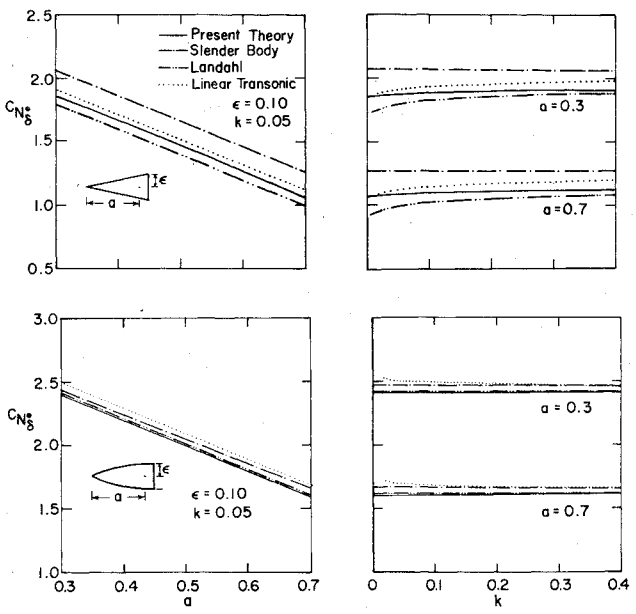

Fig. 5 Damping-in-pitch normal-force coefficient for a cone and parabolic half-body with $\epsilon = 0.1$ at $M_\infty = 1$.

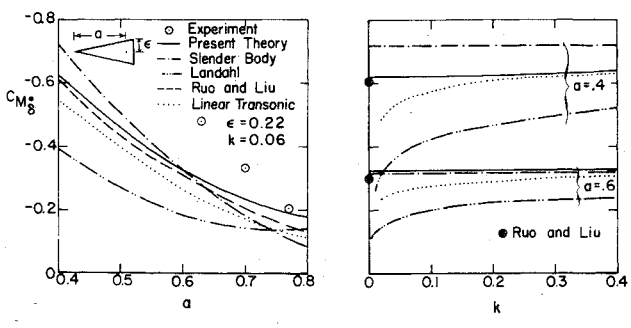

Fig. 6 Pitch axis and frequency dependence of damping-in-pitch moment coefficient of a 12.5 deg half-angle cone at $M_\infty = 1$.

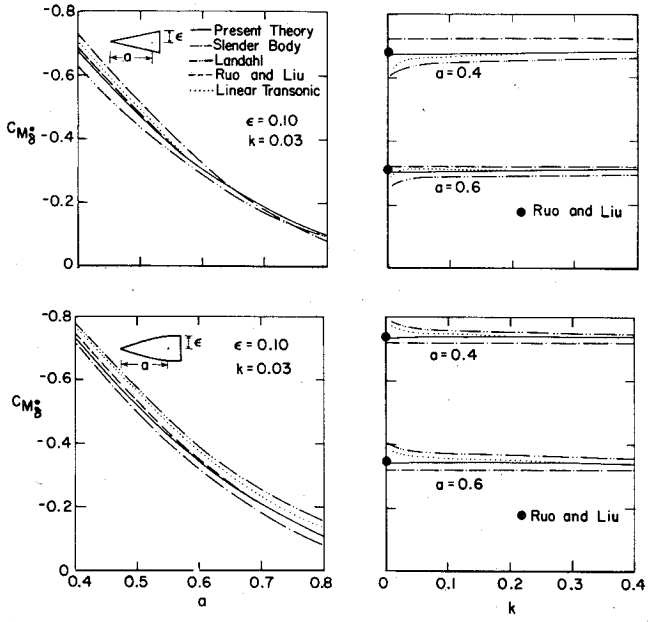

Fig. 7 Damping-in-pitch moment coefficient for a cone and parabolic half-body with $\epsilon = 0.1$ at $M_\infty = 1$.

cies and note the smooth variation with frequency of the present results.

Finally, an assessment of the effect of body shape on C_{M_δ} is provided in Fig. 7, which compares the pitch axis and frequency dependence for a cone and parabolic half-body with $\epsilon = 0.10$ at $M_\infty = 1$. We note in these results the relative closeness of the different methods for both the cone and parabolic half-body.

Concluding Remarks

In this paper, we have given an account of a theoretical study to calculate unsteady surface pressure distributions and stability derivatives for slender, pointed, axisymmetric bodies undergoing low-frequency pitching oscillations in a flow with sonic or near-sonic freestream velocity. The results are shown to be in good agreement with the limited experimental data available for comparison. Additional testing is needed, particularly for the dynamic derivatives, to provide a definitive evaluation of the theoretical predictions.

Finally, we note that the local linearization procedures by which the solutions have been obtained are not restricted to the particular examples displayed in this paper but possess greater generality. The present results, in fact, provide yet another application of the method demonstrating the remarkable ability of the technique to obtain both an accurate and economical approximation to a difficult nonlinear problem.

References

[1] Landahl, M. T., "Forces and Moments on Oscillating Slender Wing-Body Combinations at Sonic Speed," Air Force Office of Scientific Research, Washington, D.C., OSR TN No. 56-109, 1956.

[2] Liu, D. D., "Quasi-Slender Body Theory for Unsteady Linearized Transonic Flow Past Pointed Bodies of Revolution," LSMC/HREC A79 1435, 1968.

[3] Liu, D. D., Platzer, M. F., and Ruo, S. Y., "On the Calculation of Static and Dynamic Stability Derivatives for Bodies of Revolution at Subsonic and Transonic Speeds," AIAA Paper 70-190, New York, 1970.

[4] Ruo, S. Y. and Liu, D. D., "Calculation of Stability Derivatives for Slowly Oscillating Bodies of Revolution at Mach 1.0," LSMC/HREC DI 62375, 1971.

[5] Isogai, K., "A Method for Predicting Unsteady Aerodynamic Forces on Oscillating Wings with Thickness in Transonic Flow Near Mach 1," National Aerospace Lab., Tokyo, Japan, TN NAL-TR-368T, June 1974.

[6] Dowell, E. H., "A Simplified Theory for Oscillating Airfoils in Transonic Flow," *Unsteady Aerodynamics—Proceedings of a Symposium*, University of Arizona, Vol. 2, 1975, pp. 655-680.

[7] Platzer, M. F. and Hoffman, G. H., "Quasi-Slender Body Theory for Slowly Oscillating Bodies of Revolution in Supersonic Flow," NASA TN D-3440, June 1966.

[8] Stahara, S. S. and Spreiter, J. R., "Unsteady Local Linearization Solution for Pulsating Bodies at $M_\infty = 1$," *AIAA Journal*, Vol. 14, July 1976, pp. 990-992.

[9] Abramowitz, M., and Stegun, I. A., *Handbook of Mathematical Functions*, National Bureau of Standards, 1966, p. 228.

[10] Spreiter, J. R. and Alksne, A., "Slender Body Theory Based on Approximate Solution of the Transonic Flow Equation," NASA TR R-2, 1959.

[11] Wehrend, W., Jr., "An Experimental Evaluation of Aerodynamic Damping Moments of Cones with Different Center of Rotation," NASA TN D-1768, 1963.